Supporting Information

Experimental Section

Synthetic Procedure

Benzenecarboxylic acid (PhCOOH) was purchased from Acros Organics and used without further purification. Hexanuclear dysprosium complex of general formula $[Dy_6O(OH)_8(NO_3)_6(H_2O)_{12}]\cdot 2NO_3\cdot 2H_2O$ was synthesized according to previously reported methods.[1-4] 500 mg (0.27 mmol) of hexanuclear dysprosium complex were dissolved in ethylene glycol (10 mL). A saturated solution of HPhCOO in ethylene glycol (10 mL) was added and the reaction mixture was stirred for 2h at 50°C. During heating, precipitation occurred and a microcrystalline powder of $\{Dy(PhCOO)_3(EG)\}_n$ was obtained. The filtrate was evaporated at 60°C during several weeks to afford single crystals suitable for X-Ray single crystal structure determination. Similar crystals have been obtained but starting from stoichiometric amounts of $DyCl3._6H_2O$ and PhCOOH.

Crystal Structure Determination

Single crystal was mounted on an APEXII AXS-Bruker diffractometer equipped with a CCD camera and a graphite-monochromated MoKα radiation source (λ=0.71073 Å), from the Centre de Diffractométrie (CDFIX), Université de Rennes 1, France. Data were collected at 150K. Structure was solved with a direct method using the SIR-97 program[5] and refined with a full-matrix least-squares method on F^2 using the SHELXL-97 program[6] and WinGx interface.[7] Crystallographic data are summarized in Table S1. CCDC-1004691 contains the supplementary crystallographic data for this paper. These data can be obtained free of charge from The Cambridge Crystallographic Data Centre via www.ccdc.cam.ac.uk/data_request/cif.

X-ray Powder Diffraction

Diagrams have been collected using a Panalytical X'Pert Pro diffractometer with an X'Celerator detector. The typical recording conditions were 45kV, 40mA for Cu-Kα (λ=1.542Å), the diagrams were recorded in θ-θ mode in 60 min between 5° and 75° (8378 measurements) with a step size of 0.0084° and a scan time of 50s. The calculated patterns were produced using the Powdercell and WinPLOTR software programs.[8, 9]

Magnetic dc and ac Measurements

Samples were measured on a Quantum Design MPMS magnetometer on polycrystalline sample embedded in grease to avoid in-field orientation of the crystallites. Measurements were corrected for the diamagnetic contribution, as calculated with Pascal's constants, and for the diamagnetism of the sample holder, as independently determined.

Ab initio calculations

To properly account for the multiconfigurational nature of the 4f electrons wavefunction and the competition between spin-orbit coupling and crystal-field interactions in lanthanide-based SMM, explicitly correlated ab initio methods are required. Herein, the ab initio wavefunction-based calculations were carried out on a fragment of the $\{Dy(PhCOO)_3(EG)\}_n$ chain using the MOLCAS 7.6 package.[10] In this approach the relativistic effects are treated in two steps based on the Douglas-Kroll Hamiltonian. First, the scalar terms are included in the basis set generation and are used to determine the spin-free wavefunctions and energies in the complete active space self-consistent field (CASSCF) method.[11] Next, spin-orbit coupling is added within the restricted active space state interaction (RASSI-SO) method, which uses the spin-free wavefunctions as basis states.[12] The resulting wavefunctions and energies are used to compute the magnetic properties and the g-tensors of the lowest states from the energy spectrum using the pseudo-spin S=1/2 formalism in the SINGLE-ANISO routine.[13] In this work, the effects of dynamical correlation are neglected since CASPT2 calculations[14] do not change the relative energy of the spin-free states and the orientation of the magnetic anisotropy axis.[15, 16] Cholesky decomposition of the bielectronic integrals was employed to save disk space and speed-up the calculations.[17] The atomic positions were extracted from the X-ray crystal structure. All atoms were described by ANO-type basis sets from the ANO-RCC library.[18-20] The following contractions were used: [8s7p4d3f2g1h] for the central Dy ion, [4s3p2d] for the O atoms of the first coordination sphere, [4s3p] for the C and the remaining O atoms and [2s] for the H atoms. The active space of the self-consistent field (CASSCF) method consisted of the nine 4f electrons of the central Dy ion spanning the seven 4f orbitals. State-averaged CASSCF calculations were performed for all of the sextets (21 roots) and all of the quadruplets (224 roots) of the Dy ion. However, only 148 quadruplets were added to the 21 sextets to mix through spin-orbit coupling in RASSI-SO. Indeed, there is no need to add more quadruplet roots (or doublet roots) to converge the wavefunctions and energies of the ground multiplet ($^6H_{15/2}$) of the Dy ion. The anisotropy tensor, the energy of the eight Kramer doublets of ground spin-orbit state ($^6H_{15/2}$), as well as the temperature-dependent magnetic susceptibility and the molar magnetization at 2K are computed to support experimental results. Atomic charges were computed too using the LoProp approach.[21]

Table S1. Main crystallographic parameters for $\{Dy(PhCOO)_3(EG)\}_n$

Mol formula	$C_{23}H_{23}Dy_1O_8$
M ($g.mol^{-1}$)	589.5
Crystal system	monoclinic
Space group	P-*1* (N°2)
a[Å]	9.6458(2)
b[Å]	10.0989(3)
c[Å]	12.4871(4)
α[°]	95.43(0)
β[°]	104.58(1)
γ [°]	94.27(4
V[$Å^3$]	1157.65 (6)
Z	2
T[K]	150(2)
2θ range	4.06-54.90
Reflns collected	15495
Independent reflns	5308
Observed reflns	4665
Parameters	295
$R_{int}/R_1/\omega R^2$	0.0582/0.0377/0.1129
Goof	0.989

Table S2. Selected bond distances and angles in $\{Dy(PhCOO)_3(EG)\}_n$

Bond	Distance (Å)	Atoms	Angle (°)
Dy1-O1	2.460(3)	O5-Dy1-O2	152.69(14)
Dy1-O5	2.248(4)	O5-Dy1-O8	104.37(13)
Dy1-O2	2.266(3)	O2-Dy1-O8	81.56(12)
Dy1-O8	2.307(3)	O5-Dy1-O4	82.55(14)
Dy1-O4	2.308(3)	O2-Dy1-O4	105.23(12)
Dy1-O3	2.448(1)	O8-Dy1-O4	151.21(15)
Dy1-O7	2.456(3)	O5-Dy1-O3	135.38(14)
Dy1-O6	2.478(4)	O2-Dy1-O3	71.68(12)
Dy1-Dy1	4.821(2)	O8-Dy1-O3	79.53(12)
		O4-Dy1-O3	76.39(14)
		O5-Dy1-O7	71.96(14)
		O2-Dy1-O7	134.76(13)
		O8-Dy1-O7	76.21(13)
		O4-Dy1-O7	79.68(12)
		O3-Dy1-O7	65.86(11)
		O5-Dy1-O1	74.90(14)
		O2-Dy1-O1	80.41(12)
		O8-Dy1-O1	78.40(12)
		O4-Dy1-O1	130.02(13)
		O3-Dy1-O1	146.53(12)
		O7-Dy1-O1	131.09(11)
		O5-Dy1-O6	81.47(13)
		O2-Dy1-O6	74.41(13)
		O8-Dy1-O6	128.39(12)
		O4-Dy1-O6	79.97(13)
		O3-Dy1-O6	131.24(11)
		O7-Dy1-O6	148.27(13)
		O1-Dy1-O6	53.22(10)

Table S3. Calculation of the agreement between the coordination polyhedron of the studied complexes with various ideal polyhedra using the SHAPE program[22]

	$\{Dy(PhCOO)_3(EG)\}_n$			**DyFur**			**DyNitro**			**DyHPA**		
Ideal Polyhedron Geometry	SAP (D4d)	BTPR (C2v)	TDD (D2d)	SAP	BTPR	TDD	SAP	BTPR	TDD	SAP	BTPR	TDD
Agreement factor (the lower is the best)	2.161	2.340	2.773	2.79	2.80	4.23	2.13	2.39	2.51	5.89	3.95	3.56

*SAP= Square antiprism; BTPR= Biaugmented trigonal prism; TDD= Triangular dodecahedron

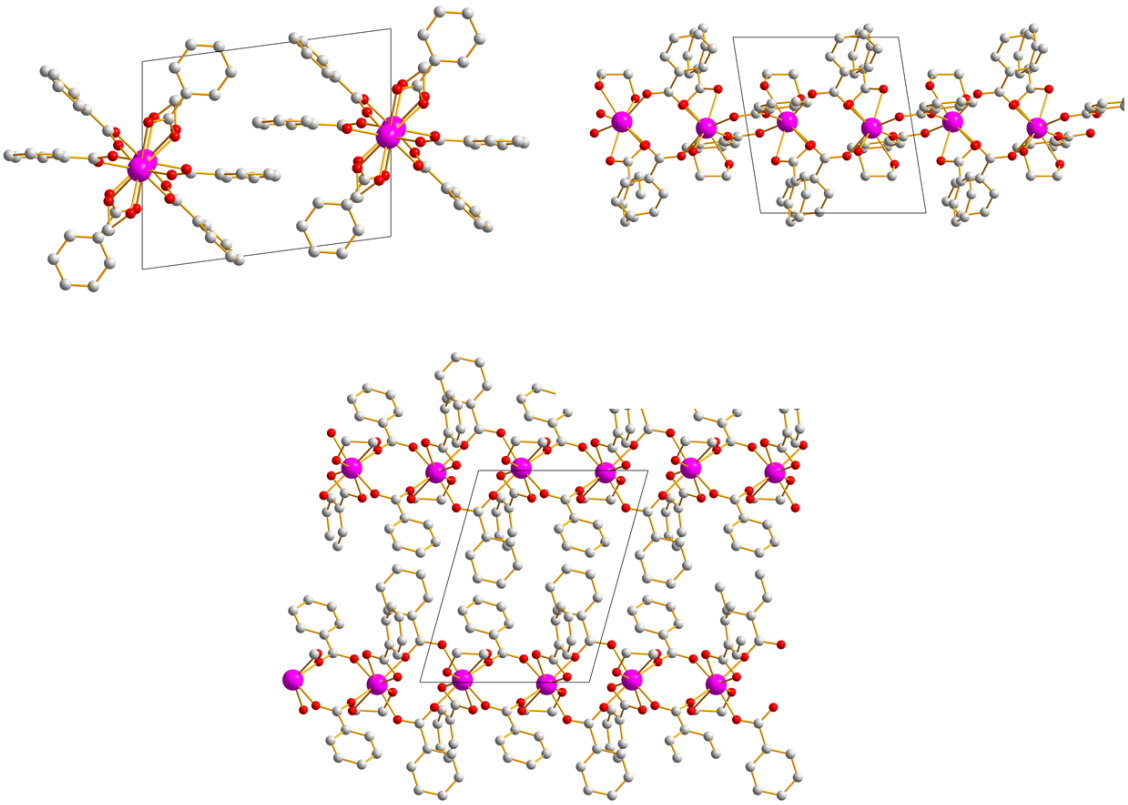

Figure S1. Representation of the arrangement of the chains in $\{Dy(PhCOO)_3(EG)\}_n$ along a (top left), c (top right) and b axes (bottom)

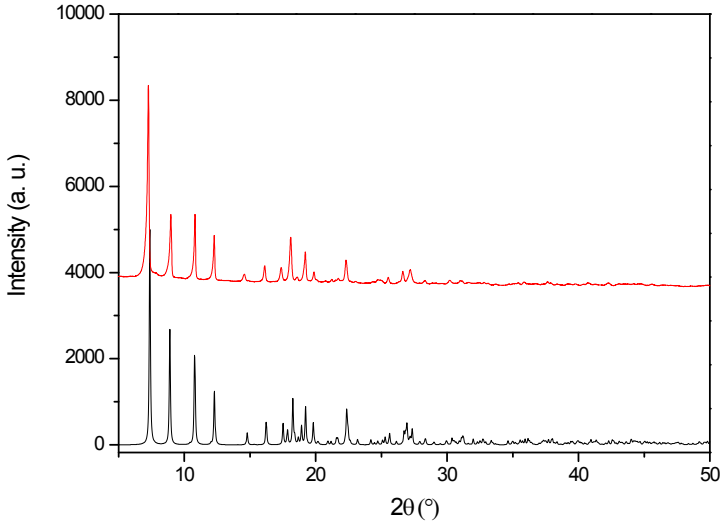

Figure S2. X-Ray diffraction powder pattern of $\{Dy(PhCOO)_3(EG)\}_n$ simulated from structural data file (.cif) at 150 K (bottom) and the $\{Dy(PhCOO)_3(EG)\}_n$ powder (top) recorded at room temperature.

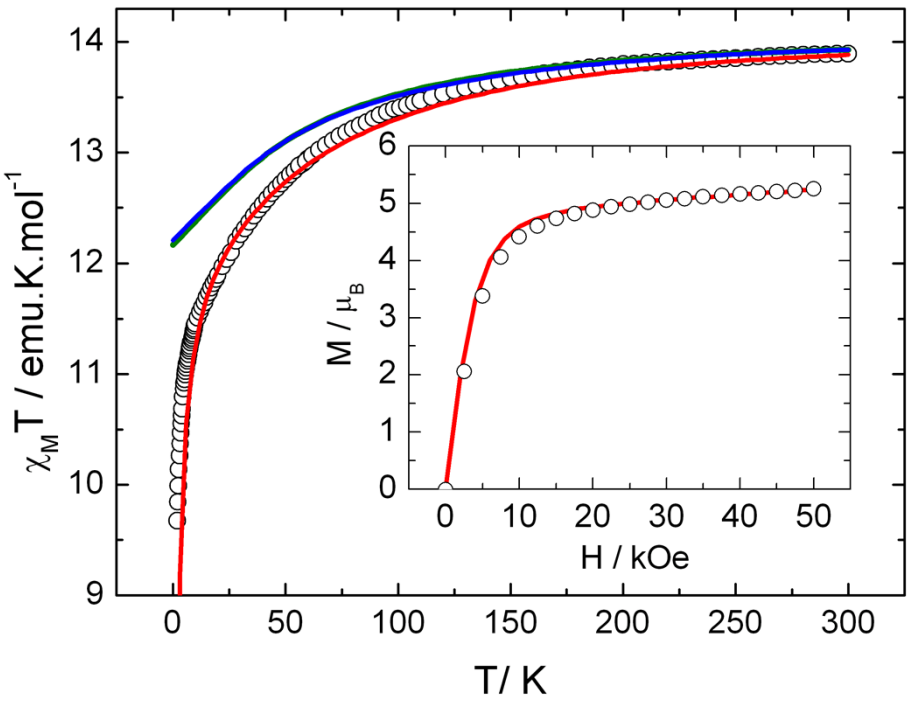

Figure S3. Temperature dependence of $\chi_M T$ (circles). Calculated curves obtained with models **A** (green), **B** (blue, almost superimposed) and **A** considering $\mathbf{J_{dd}}$ interaction (red) as determined by single crystal magnetic measurements. In inset field dependence of M measured at 2K. Calculated curve obtained with models **A** considering $\mathbf{J_{dd}}$ interaction (red)

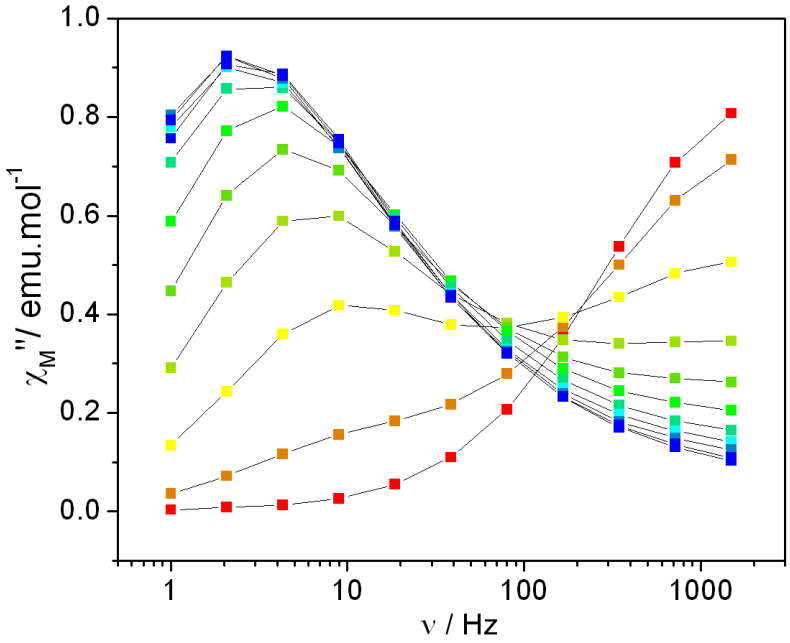

Figure S4. Frequency dependence of the out-of phase susceptibility of $\{Dy(PhCOO)_3(EG)\}_n$ at 2K with field ranging from O (red) to 2000 Oe (blue)

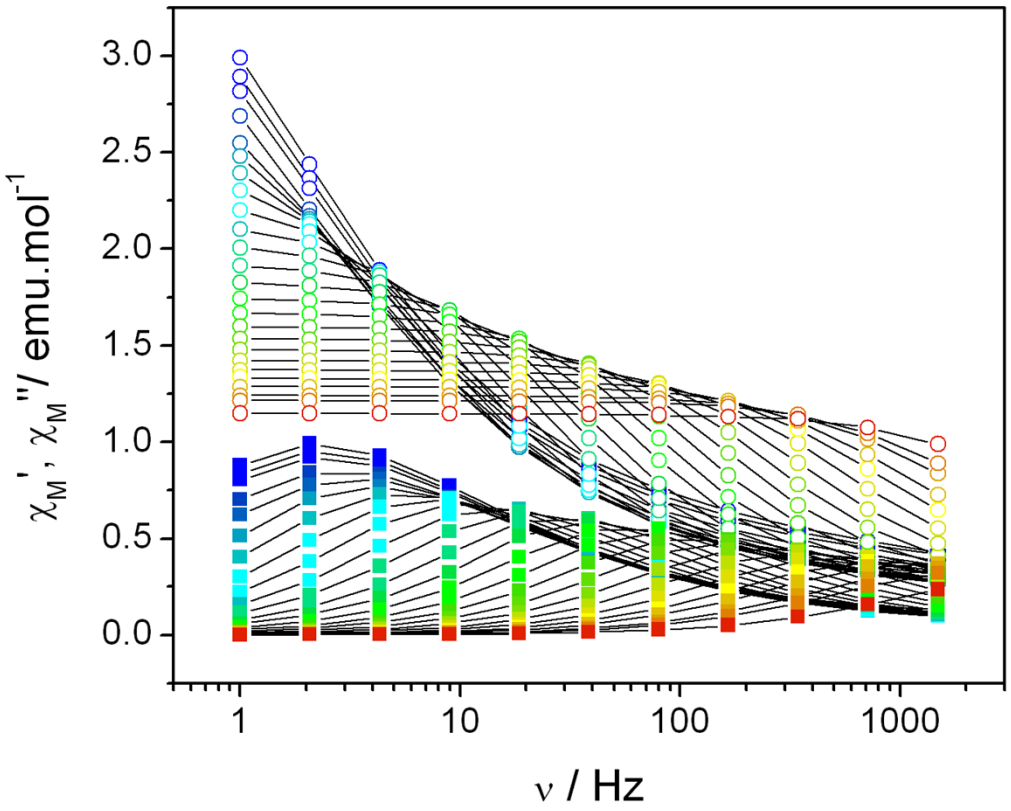

Figure S5. Frequency dependence of the in-phase (squares) and out-of phase (circles) susceptibility of $\{Dy(PhCOO)_3(EG)\}_n$ with temperature ranging from 1.8 (blue) to 8K (red) measured with a 1600 Oe external dc field.

Table S4. Extracted τ values from the fitting of *X'' vs frequency* curves in 1600 Oe dc field.

T(K)	τ (μs)	T(K)	τ (μs)	T(K)	τ (μs)
1.8	67338	3.75	9975	6	400
1.9	65103	4	7383	6.25	272
2	61327	4.25	5055	6.5	190
2.25	51240	4.5	3896	6.75	144
2.5	42416	4.75	2640	7	104
2.75	33146	5	1826	7.25	86
3	26698	5.25	1307	7.75	51
3.25	19005	5.5	923		
3.5	13985	5.75	604		

Table S5. Extracted values from the Argand plot with a 1600 Oe external field before normalization

T (K)	χ_s / emu mol^{-1}	χ_T / emu mol^{-1}	α
1.8	0.428	4.266	0.359
1.9	0.494	4.037	0.379
2	0.473	3.892	0.376
2.25	0.437	3.537	0.364
2.5	0.418	3.216	0.335
2.75	0.403	2.953	0.311
3	0.400	2.698	0.274
3.25	0.404	2.484	0.234
3.5	0.414	2.306	0.193
3.75	0.363	2.170	0.188
4	0.322	2.054	0.185
4.25	0.293	1.944	0.180
4.5	0.298	1.846	0.163
4.75	0.307	1.754	0.145
5	0.281	1.678	0.152
5.25	0.258	1.609	0.166
5.5	0.269	1.543	0.156
5.75	0.281	1.482	0.152
6	0.301	1.426	0.143
6.25	0.316	1.376	0.147
6.5	0.377	1.327	0.116
6.75	0.375	1.289	0.128
7	0.399	1.241	0.127
7.25	0.427	1.214	0.120
7.75	0.405	1.147	0.130

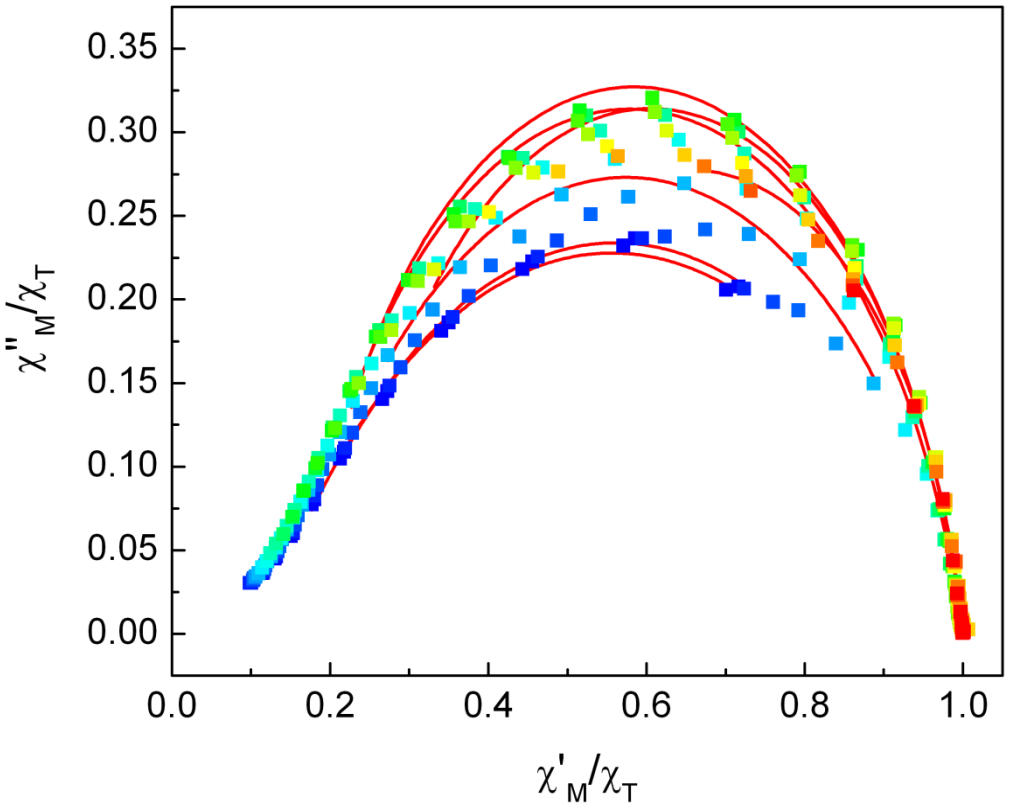

Figure S6. Argand diagram extracted from the ac measurement of $\{Dy(PhCOO)_3(EG)\}_n$ with temperature ranging from 1.8 (blue) to 8K (red) with some of the best fits.

Table S6. Energy spectrum, anisotropy tensor and easy-axis deviation for model **A** and **B** calculated on $\{Dy(PhCOO)_3(EG)\}_n$.

	Model A	Model B
Energy spectrum (cm^{-1})		
0	0	0
1	92	119
2	130	159
3	229	229
4	322	283
5	389	305
6	423	358
7	454	441
Anisotropy tensor of the ground state		
g_X	0.015	0.002
g_Y	0.026	0.005
g_Z	19.763	19.730
Deviation to the experimental magnetic easy (°)		
	9	10

Description of the other chains considered for the calculations.

$\{Dy(2\text{-fur})_3(HOCH_2CH_2OH)\}_n$, later named **DyFur** [23] is a chain very similar to the title compound. Comparing with $\{Dy(PhCOO)_3(EG)\}_n$, PhCOO ligands are replaced by 2-furoate ligands. Dy-Dy distances are 5.053 Å and 4.619 Å. Coordination polyhedron can be described either as a square antiprism or a biaugmented trigonal prism (same SHAPE agreement factors: 2.80; see table S3).

$\{Dy(4\text{-methyl-3-nitrobenzoate})_3(H_2O)(CH_3OH)\}_n$, later named **DyNitro** [24] is a chain where PhCOO liagnds are changed for 4-methyl-3-nitrobenzoate, and ethyleneglycol is substituted by one methanol and one water molecule. Dy-Dy distances are 4.889 Å and 4.955 Å. Coordination polyhedron can be described as a similar square antiprism as in $\{Dy(PhCOO)_3(EG)\}_n$.

$\{[Dy(HPA)_2(NO3)_2]NO_3\}_n$, later named **DyHPA**,[25] is a chain where PhCOO is substituted by 4-pyridylthioacetic ligands. Capping ethyleneglycol and carboxylate are substituted by chelating nitrate anions. Dy-Dy distance is 5.140 Å. Coordination polyhedron is very far from any ideal shape and can be best described as triangular dodecahedron.

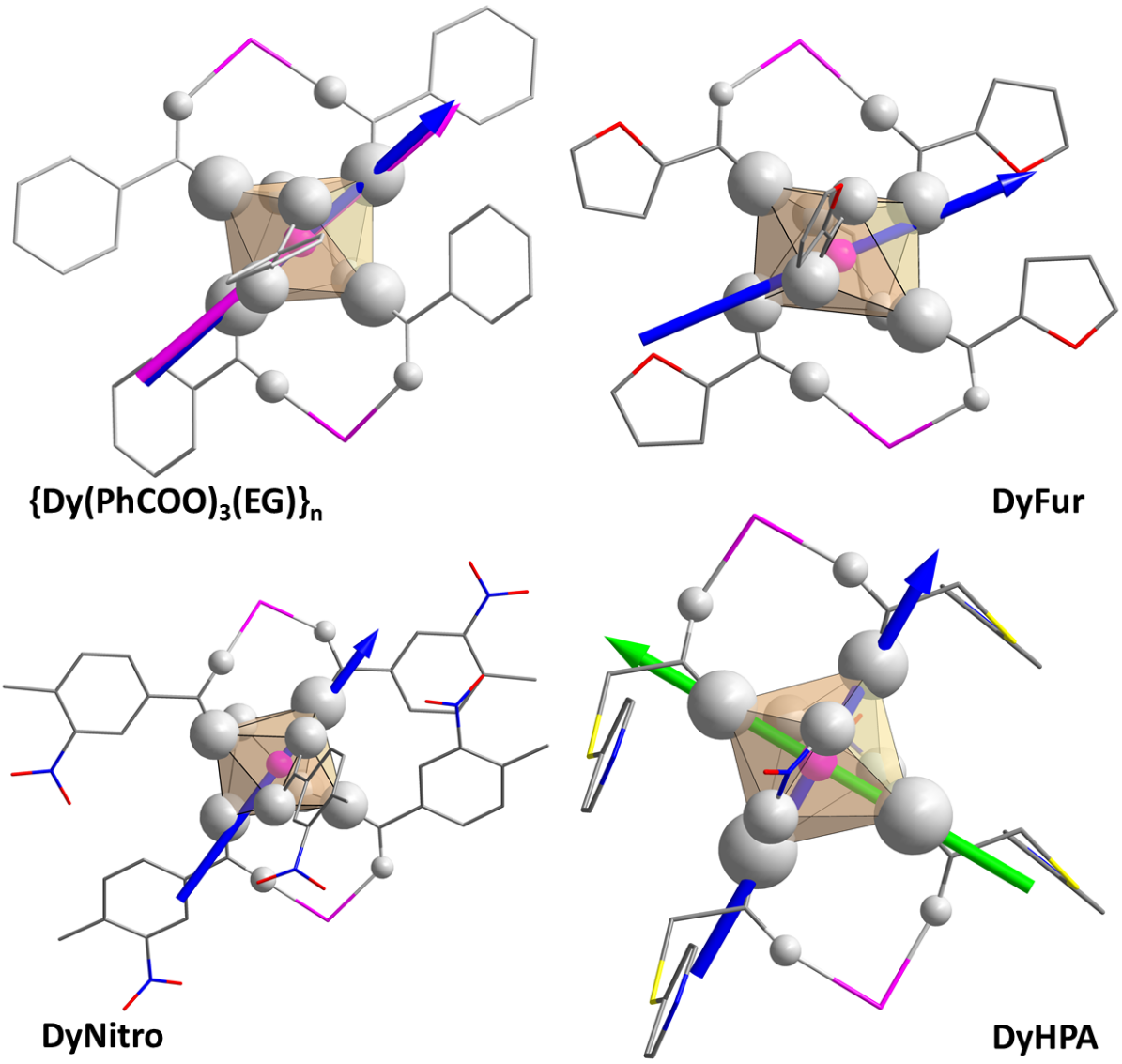

Figure S7 : Representation perpendicular to the chain direction of calculated ground state anisotropy axes for $\{Dy(PhCOO)_3(EG)\}_n$, DyFur, DyNitro and DyHPA in blue (for DyHPA first excited state anisotropy axis in green). Fragments are depicted with potential of oxygen with respect to the Dy^{III} ion as grey balls.

Table S7. Energy spectrum and anisotropy tensor computed for all chains with model **A**.

	$\{Dy(PhCOO)_3(EG)\}_n$	DyFur	DyNitro	DyHPA
Energy spectrum (cm^{-1})				
0	0	0	0	0
1	92	170	172	10
2	130	320	209	123
3	229	354	304	184
4	322	438	368	293
5	389	466	418	414
6	423	555	435	431
7	454	683	467	541
Anisotropy tensor of the ground state				
g_X	0.015	0.003	0.125	0.001
g_Y	0.026	0.003	3.568	0.001
g_Z	19.763	19.849	15.639	19.745

$\{[Dy(bza)_3EG]_2\}_n$				DyFur				DyNitro				DyHPA			
	Distance Dy-O (Å)	**Charge**	**Potential* (a.u.)**		**Distance Dy-O (Å)**	**Charge**	**Potential* (a.u.)**		**Distance Dy-O (Å)**	**Charge**	**Potential* (a.u.)**		**Distance Dy-O (Å)**	**Charge**	**Potential* (a.u.)**
$O_{bridging}$	2.27	-0.81	0.19	$O_{bridging}$	2.40	-0.86	0.19	$O_{bridging}$	2.20	-0.85	0.20	$O_{bridging}$	2.27	-0.86	0.20
$O_{bridging}$	2.24	-0.81	0.19	$O_{bridging}$	2.18	-0.76	0.18	$O_{bridging}$	2.29	-0.80	0.18	$O_{bridging}$	2.27	-0.85	0.20
$O_{bridging}$	2.31	-0.82	0.19	$O_{bridging}$	2.38	-0.85	0.19	$O_{bridging}$	2.34	-0.80	0.18	$O_{bridging}$	2.26	-0.76	0.18
$O_{bridging}$	2.31	-0.83	0.19	$O_{bridging}$	2.24	-0.75	0.18	$O_{bridging}$	2.30	-0.82	0.19	$O_{bridging}$	2.26	-0.76	0.18
$O_{capping\text{-}carbox}$	2.46	-0.74	0.16	$O_{capping\text{-}carbox}$	2.38	-0.77	0.17	$O_{capping\text{-}carbox}$	2.47	-0.73	0.16	$O_{capping\ NO3}$	2.43	-0.64	0.14
$O_{capping\text{-}carbox}$	2.48	-0.74	0.16	$O_{capping\text{-}carbox}$	2.53	-0.68	0.14	$O_{capping\text{-}carbox}$	2.47	-0.74	0.16	$O_{capping\ NO3}$	2.43	-0.64	0.14
$O_{capping\text{-}EG}$	2.44	-0.60	0.13	$O_{capping\text{-}EG}$	2.56	-0.59	0.12	O_{H2O}	2.41	-0.73	0.16	$O_{capping\ NO3}$	2.47	-0.59	0.13
$O_{capping\text{-}EG}$	2.45	-0.60	0.13	$O_{capping\text{-}EG}$	2.43	-0.61	0.13	$O_{methanol}$	2.47	-0.66	0.14	$O_{capping\ NO3}$	2.47	-0.59	0.13
$O_{bridging\ Dy'}$	3.49	-0.65	0.10	$O_{bridging\ Dy'}$	3.28	-0.73	0.12	$O_{bridging\ Dy'}$	3.57	-0.66	0.10	$O_{bridging\ Dy'}$	3.87	-0.58	0.08
$O_{bridging\ Dy'}$	3.55	-0.66	0.10	$O_{bridging\ Dy'}$	3.38	-0.70	0.11	$O_{bridging\ Dy'}$	3.79	-0.68	0.09	$O_{bridging\ Dy'}$	3.87	-0.58	0.08
$O_{bridging\ Dy'}$	4.29	-0.70	0.09	$O_{bridging\ Dy'}$	4.56	-0.62	0.07	$O_{bridging\ Dy'}$	4.32	-0.69	0.08	$O_{bridging\ Dy'}$	4.04	-0.69	0.09
$O_{bridging\ Dy'}$	4.33	-0.70	0.09	$O_{bridging\ Dy'}$	4.57	-0.65	0.08	$O_{bridging\ Dy'}$	4.17	-0.66	0.08	$O_{bridging\ Dy'}$	4.04	-0.69	0.09
Dy		2.569				2.568				2.577				2.567	

$O_{brindging}$: Oxygen atoms. from a carboxylate ligand that bridges two Dy^{III} ions. and linked to the central Dy^{III} .

$O_{brindging\ Dy'}$: Oxygen atoms. from a carboxylate ligand that bridges two Dy^{III} ions. and linked to another Dy^{III} .

$O_{capping}$: Oxygen atoms that cap a Dy^{III}. and so are not in the chain direction

*Potentials are calculated as q/r. where q is the atomic charge and r the distance between the Dy and the O atoms.

1 G. Calvez, O. Guillou, C. Daiguebonne, P. E. Car, V. Guillerm, Y. Gerault, F. Le Dret and N. Mahe, *Inorg. Chim. Acta*, 2008, **361**, 2349-2356.

2 O. Guillou, C. Daiguebonne, G. Calvez, F. Le Dret and P. E. Car, *J. Alloys Compd.*, 2008, **451**, 329-333.

3 G. Calvez, C. Daiguebonne, O. Guillou and F. Le Dret, *Eur. J. Inorg. Chem.*, 2009, 3172-3178.

4 G. Calvez, C. Daiguebonne, O. Guillou, T. Pott, P. Meleard and F. Le Dret, *C. R. Chim.*, 2010, **13**, 715-730.

5 A. Altomare, M. C. Burla, M. Camalli, G. L. Cascarano, C. Giacovazzo, A. Guagliardi, A. G. G. Moliterni, G. Polidori and R. Spagna, *J. Appl. Crystallogr.*, 1999, **32**, 115-119.

6 G. M. Sheldrick and T. R. Schneider, *Methods Enzymol.*, 1997, **277**, 319-343.

7 L. Farrugia, *J. Appl. Crystallogr.*, 1999, **32**, 837-838.

8 T. Roisnel and J. Rodriguez-Carvajal, in *Epdic 7: European Powder Diffraction, Pts 1 and 2*, eds. R. Delhez and E. J. Mittemeijer, Trans Tech Publications Ltd, Zurich-Uetikon, 2001, pp. 118-123.

9 W. Kraus and G. Nolze, *J. Appl. Crystallogr.*, 1996, **29**, 301-303.

10 F. Aquilante, L. De Vico, N. Ferre, G. Ghigo, P. Å. Malmqvist, P. Neogrady, T. B. Pedersen, M. Pitonak, M. Reiher, B. O. Roos, L. Serrano-Andres, M. Urban, V. Veryazov and R. Lindh, *J. Comput. Chem.*, 2010, **31**, 224-247.

11 B. O. Roos, P. R. Taylor and P. E. M. Siegbahn, *Chem. Phys.*, 1980, **48**, 157-173.

12 P. Å. Malmqvist, B. O. Roos and B. Schimmelpfennig, *Chem. Phys. Lett.*, 2002, **357**, 230-240.

13 L. F. Chibotaru and L. Ungur, *J. Chem. Phys.*, 2012, **137**.

14 K. Andersson, P. Å. Malmqvist and B. O. Roos, *J. Chem. Phys.*, 1992, **96**, 1218-1226.

15 G. Cosquer, F. Pointillart, J. Jung, B. Le Guennic, S. Golhen, O. Cador, Y. Guyot, A. Brenier, O. Maury and L. Ouahab, *Eur. J. Inorg. Chem.*, 2014, **2014**, 69-82.

16 T. T. da Cunha, J. Jung, M. E. Boulon, G. Campo, F. Pointillart, C. L. M. Pereira, B. Le Guennic, O. Cador, K. Bernot, F. Pineider, S. Golhen and L. Ouahab, *J. Am. Chem. Soc.*, 2013, **135**, 16332-16335.

17 F. Aquilante, P. Å. Malmqvist, T. B. Pedersen, A. Ghosh and B. O. Roos, *J. Chem. Theory Comput.*, 2008, **4**, 694-702.

18 B. O. Roos, R. Lindh, P. Å. Malmqvist, V. Veryazov, P. O. Widmark and A. C. Borin, *J. Phys. Chem. A*, 2008, **112**, 11431-11435.

19 B. O. Roos, R. Lindh, P. Å. Malmqvist, V. Veryazov and P. O. Widmark, *J. Phys. Chem. A*, 2005, **109**, 6575-6579.

20 P. O. Widmark, P. Å. Malmqvist and B. O. Roos, *Theor. Chim. Acta*, 1990, **77**, 291-306.

21 L. Gagliardi, R. Lindh and G. Karlstrom, *J. Chem. Phys.*, 2004, **121**, 4494-4500.

22 S. Alvarez, P. Alemany, D. Casanova, J. Cirera, M. Llunell and D. Avnir, *Coord. Chem. Rev.*, 2005, **249**, 1693-1708.

23 E. Bartolome, J. Bartolome, S. Melnic, D. Prodius, S. Shova, A. Arauzo, J. Luzon, F. Luis and C. Turta, *Dalton Trans.*, 2013, **42**, 10153-10171.

24 J. M. Tian, B. Li, X. Y. Zhang, X. L. Li, X. L. Li and J. P. Zhang, *Dalton Trans.*, 2013, **42**, 8504-8511.

25 Y. Wang, X.-L. Li, T.-W. Wang, Y. Song and X.-Z. You, *Inorg. Chem.*, 2009, **49**, 969-976.